An Undulation Theory for Condensation in Open End Slit Pores:

Critical Hysteresis Temperature & Critical Hysteresis Pore Size

by

Chunyan Fan[1], Yonghong Zeng[2], D. D. Do*[2] and D. Nicholson[2]

[1]Department of Chemical Engineering
Curtin University
Bentley, WA 6845, Australia

[2]School of Chemical Engineering
University of Queensland
St. Lucia, Qld 4072, Australia

Abstract

A new theory of condensation in an open end slit pore, based on the concept of temperature dependent undulation, at the interface separating the adsorbed phase and the gas-like region, is presented. The theory, describes, for the first time, the microscopic origin of the critical hysteresis temperature and the critical hysteresis pore size, properties which are not accessible to any classical theories.

* Author to whom all correspondence should be addressed. Email: d.d.do@uq.edu.au

1. Introduction

Adsorption isotherms of gases in mesoporous solids exhibit hysteresis at temperatures below a critical hysteresis temperature, above which the adsorption isotherm is reversible [1-4]. Hysteresis has become a subject of great interest to adsorption scientists and engineers especially because of the advances in synthesis of ordered mesoporous materials [5, 6], which can be tailored, and are sufficiently well structured for the fundamental study of the phenomena of condensation and evaporation.

Adsorption in mesoporous solids is often modelled using simple pore models, typically slits or cylinders with both ends open to the gas phase. The classical view of hysteresis originates from the work of Cohan [7], who argued that adsorption and desorption in a cylindrical pore followed different paths because of the difference in the curvature (cylindrical on adsorption and spherical on desorption) of the meniscus separating the adsorbed phase and the gas-like phase. This simplified view cannot explain why hysteresis disappears as temperature is increased and moreover the Cohan-Kelvin model takes no account of the external adsorbent field. Several subsequent theories have attempted to remedy the latter defect by accounting for the influence of the surface force from the adsorbent; Schuchowitzki and Derjaguin were the first to study the contribution from this to capillary condensation [8, 9], and it was considered later by Broekhoff and de Boer [10-14] and in the statistical theory of Cole and Saam [15].

Everett and Haynes developed a more general thermodynamic theory for hysteresis in cylinders, in which critical curvature could arise in a third way through the establishment of an unduloidal interface [16]. However, none of these theories offer a mechanism for hysteresis in slit pores, evidence for which is well established from molecular simulation [17-21] and from experimental studies of adsorption in adsorbents with lamellar structure. Several theoretical studies have also confirmed that hysteresis does occur in pores with slit-shaped geometry: for example the lattice gas model of Marconi and van Swol [22, 23], density functional theories pioneered by Evans et al. [4, 24], and by Balbuena and Gubbins [25] and the gauge-cell method used by Jorge and Seaton [26].

Gas adsorption in simple pore models such as slits or cylinders is usually explained as a process of two sequential steps: molecular layering on the pore wall, followed by condensation when the gas-like core has become sufficiently narrow. This general picture is supported by several computational studies [17, 20, 22, 27]. Recent experimental and simulation

investigations of the effects of temperature on adsorption in open ended pores have provided several interesting observations: (1) the reduced pressure at condensation shifts to a lower value as temperature is increased while reduced pressure at evaporation shifts to a higher value, resulting in a smaller hysteresis loop, (2) the magnitude of the steep change in the adsorbed density at condensation and the adsorbed density just before condensation is smaller at higher temperatures and (3) the hysteresis loop disappears at a so-called critical hysteresis temperature (T_{ch}), but a sharp jump in density is still observed and the jump is smaller with temperature until the temperature reaches the pore critical temperature (T_{cp}). A search for the molecular mechanisms underlying these observations in slit shaped pores is the objective of this paper.

2. Theory

2.1 Grand Canonical Monte Carlo simulation

We used argon as a model adsorbate with an intermolecular potential energy of interaction described by the 12-6 Lennard-Jones (LJ) equation with σ_{ff}= 0.3405 nm and ε_{ff}/k = 119.8 K. The slit pore model was constructed from graphitic walls that are finite in the *y*-direction and infinite in the *x*-direction. The solid-fluid potential energy was calculated from the Bojan-Steele equation [28-30]. The pore walls consisted of three homogeneous layers of constant surface density ρ_s= 38.2 nm^{-2} and a spacing Δ=0.3354 nm. The molecular parameters for a carbon atom in a layer were: σ_{ss}= 0.34 nm and ε_{ss}/k = 28 K. The cross collision diameter and well-depth of the solid-fluid interaction energy were calculated by the Lorentz-Berthelot mixing rule.

GCMC simulations were run with 100,000 cycles for both the equilibration and sampling stages. Each cycle consisted of 1000 displacement moves and exchanges, which included insertion and deletion, with equal probability. For each simulation, we collected control charts, of the running mean of the ensemble averages of the configuration energy and the particle number, to monitor convergence to equilibrium. In the equilibration stage, the maximum displacement length was initially set as half of the largest dimension of the box and was adjusted at the end of each cycle to give an acceptance ratio for displacement of 20% [31, 32]. The length of the simulation box in the *x*-direction was 10 times the collision diameter of argon, and the lengths of the other two directions were determined by the pore dimensions. The gas reservoir had a length of 3nm along the pore axis, and the dimensions in the other two directions were the same as those of the pore. Periodic boundary conditions were applied

at the boundaries in the *x*-direction, and the cut-off radius was 5 times the collision diameter. For a given pressure, the chemical potential was calculated from the equation of state of Johnson *et al*. [33] and was used as the input in GCMC simulation.

To examine mass transfer in the adsorbed layer in more detail, we collected particle number fluctuations defined as:

$$\frac{f(N,N)}{\langle N \rangle} = \frac{\langle N^2 \rangle - \langle N \rangle^2}{\langle N \rangle}$$

The pore space was divided into bins along the pore, and the local number fluctuation in each bin was calculated. The particle number fluctuation would be unity in an ideal gas bin [34].

3. Results and Discussion

3.1 Argon Adsorption in 3nm Pore

For a given slit of uniform width and finite length, we carried out GCMC simulations to obtain adsorption isotherms at each temperature and pore width. The adsorption isotherm for argon at 87 K in a pore of width 3 nm and length 14 nm is shown in Figure 1. As expected for a uniform slit pore, the hysteresis loop is type H1, however, an interesting feature that is worth noting is the gap between the adsorption and desorption branches after condensation, i.e. from point D onwards. This gap indicates that the condensed fluid inside the pore is more cohesive during desorption than that during adsorption, i.e. after the fluid has condensed at point D, it is restructured to optimise the molecular packing while the two interfaces proceed to the pore mouths and eventually fill the pore.

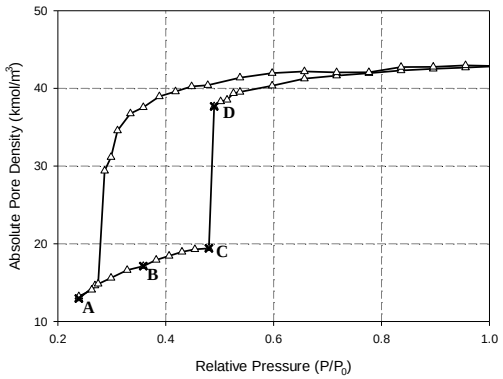

Figure 1: Adsorption isotherm of argon at 87 K in a slit pore of width 3 nm and length 14 nm. The saturation pressure used in this work is calculated based on the equation developed by Lotfi et al. [35]

The singlet particle density distribution $\rho(z)$ as a function of the distance from one of the pore walls is shown in Figure 2 for the pressure points (A, B and C) indicated in Figure 1,

together with the corresponding particle number fluctuation (PNF). From this plot we can identify two distinct regions: a region of "dense" adsorbed layer (I), where the PNF is less than unity, and a fluctuation region (II), the PNF is greater than unity; this indicates that there is considerable freedom of movement of the molecules, and that there is frequent mass exchange between the adsorbed phase and the gas-like phase [34].

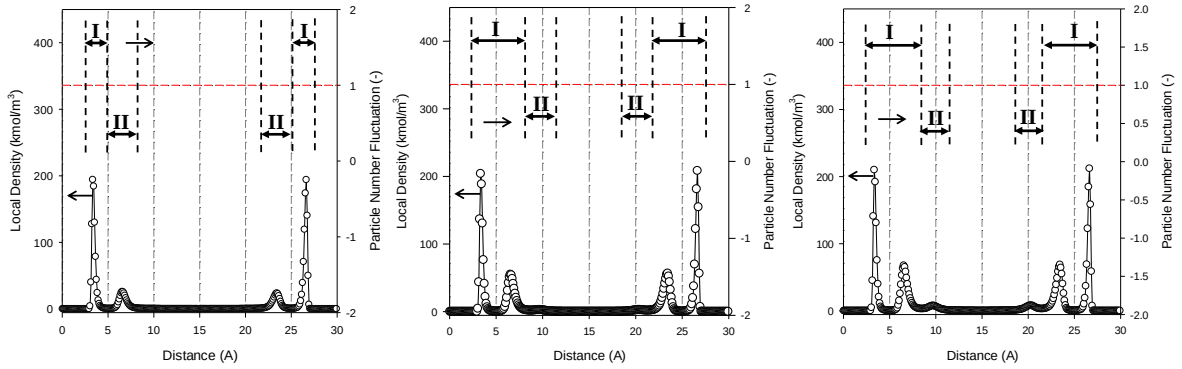

Figure 2: Local density distribution (circles) and particle number fluctuation (solid lines) as a function of distance from a wall for argon adsorption at 87 K in a slit pore of width 3 nm and length 14 nm, for the three pressure points labelled in Figure 1.

The dense adsorbed layer here refers to the area under $\rho(z)$ where the PNF is <1 and not to the total area under $\rho(z)$ which includes second and higher layers that may contribute to a statistical monolayer. The region of the statistical monolayer does not reveal its microscopic behaviour, but as will be shown below the PNF highlights the important influence of temperature on the behaviour of the adsorbed phase.

Adsorption proceeds by molecular layering on the pore walls (points A, B and C in Figure 1) as the pressure increases up to point C. The thickness of the dense adsorbed layer (region I) increases with pressure, and as a consequence the fluctuation region (region II) moves away from the pore walls. The movement of molecules in and out of this region creates a diffuse interface which has on average a wave-like structure and provides a microscopic basis for the concept of an unduloid interface discussed by Everett and Haynes in 1972 [16]. For a given temperature, the dense adsorbed layer advances, and the core region becomes smaller as pressure is increased. This core region is gas-like, as seen from the PNF close to unity in Figure 2.

Figure 3 shows the thickness of the two dense adsorbed layers combined and that of the two fluctuation zones combined as a function of reduced pressure before condensation occurs.

The PNF plots at various pressures, from which the plots in Figure 3 are extracted, are given in Appendix 1.

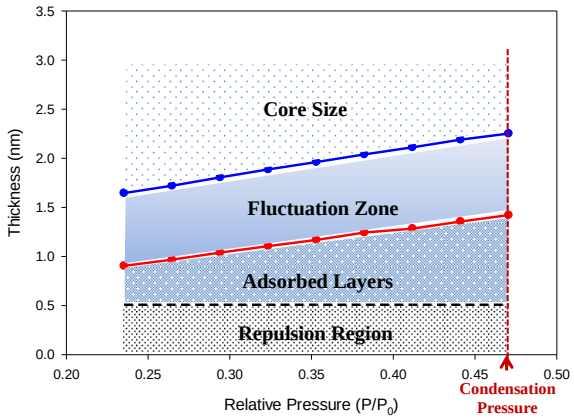

Figure 3: The thickness of the dense adsorbed layer and that of the fluctuation zone as a function of pressure for adsorption of argon at 87 K in slit pore with width of 3 nm and length of 14 nm, the values shown in this plot are the sum of the thickness from two walls except for the core size.

In this figure, the horizontal line at 3nm is drawn at the physical pore width. The region below the dashed line is close to the pore walls and is inaccessible to adsorbate because of the strong repulsion between the adsorbate and the solid. The thickness of the dense adsorbed layers on each wall increases with pressure, and as a consequence, the width of the gas-like core is reduced and is found to be about 0.76 nm at condensation. Hereafter, we refer to the position demarcating the fluctuation layer and the inner core as the fluctuation front.

If we denote the width of the dense adsorbed layer as d_A and that of the fluctuation zone as d_F, then the width of the gas-like core is given by

$$H_C = H - 2(d_A + d_F) \qquad (1)$$

where H is the physical pore width, defined as the distance from the plane passing through carbon atoms in the outermost layer of one wall to the corresponding plane on the opposite wall. At the condensation pressure the average size of the gas-like core is H_C^* =0.76 nm, and when a molecule is inserted into the core, it will interact strongly with molecules in the two opposing fluctuation zones because this is the centre to centre distance between the outer molecules in a triplet of argon molecules separated by $2^{1/6}\sigma_{ff}$, which is the pairwise separation distance at which the potential energy is minimum. This separation is the critical value for the onset of condensation. Figure 4 shows a snapshot taken from the simulation at a pressure just before condensation, showing the initiation of a liquid bridge joining the

opposing adsorbed layers. To our knowledge this is the first time that a microscopic explanation has been offered for the mechanism of condensation in a pore.

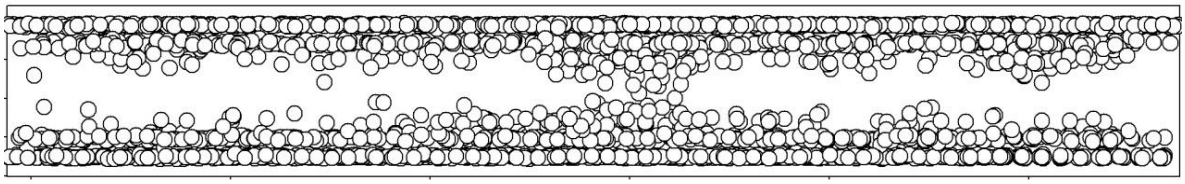

Figure 4: Snapshot of argon molecule at the point just prior to condensation at 87 K for the pore with 3 nm width and 20 nm length.

Figure 4 also illustrates the undulatory structure of the interface in the fluctuation zone which is in accord with the concept of an unduloid interface proposed by Everett and Haynes [16]. Figure 5 is a schematic diagram showing the various adsorbate regions in the pore: the dense adsorbed layer, the fluctuation zone and the gas-like core. Since this new concept involves unduloid interfaces from the two opposing walls, we shall call our theory the undulation theory.

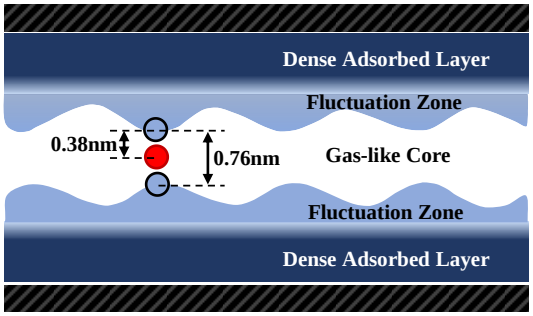

Figure 5: The schematic diagram of various phases inside the pore.

Thus we can define the sufficient condition for the condensation as:

$$[H_C = H - 2(d_A + d_F)]_{P_{cond}} = H_C^* \qquad (2)$$

where P_{cond} is the condensation pressure.

3.2 Effects of Temperature

The thickness of the fluctuation region increases with increasing temperature, therefore for a given pore size the condition for condensation in eq. (2) can be satisfied by a smaller thickness of the adsorbed layer at higher temperatures. This means that the reduced pressure and the loading just prior to condensation are lower at higher temperatures, as seen in the

isotherms in Figure 6a for the pore of 3 nm width and 14 nm length. Figure 6b shows the corresponding particle number fluctuation versus distance at the pressure just prior to condensation. The pattern of the PNF is fairly insensitive to temperature. This suggests that eq. (2) may be valid for all temperatures, and is therefore suitable for the determination of the critical hysteresis temperature, provided that we know the thickness of the adsorbed layer as a function of temperature and pressure, and the thickness of the fluctuation zone as a function of temperature. These can be obtained from simulations on a flat surface (see Section 3.6).

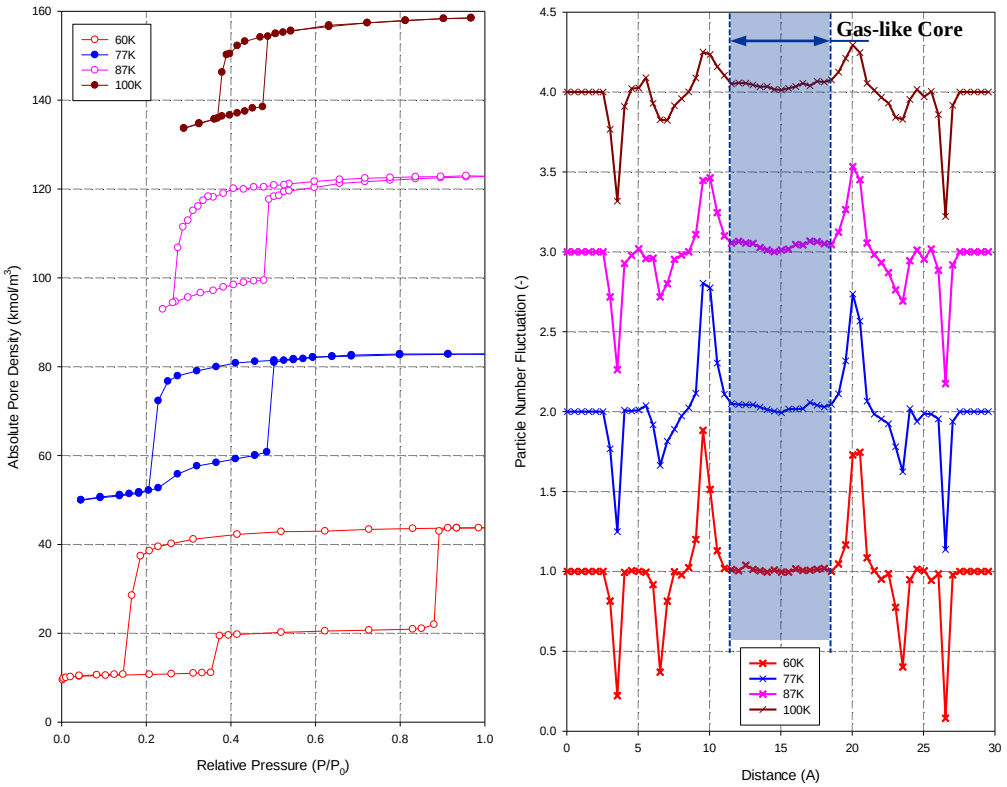

(a) (b)

Figure 6: (a) Argon adsorption isotherms in a slit pore of width 3 nm and length 14 nm from 60 K to 100 K; the saturation vapour pressure is calculated from [35], (b) the PNF just before condensation at various temperatures as a function of distance, the curves are shifted by every 40 kmol/m^3 and 1.0 for isotherms and PNF, respectively.

The thickness of the dense adsorbed layer and that of the fluctuation zone just before condensation for the 3 nm pore width are shown as a function of temperature in Figure 7a. Also plotted in the same figure is the reduced condensation pressure versus temperature. We see that the width of the fluctuation zone increases while that of the adsorption layer decreases, with increasing temperature. The same results for the 4 nm pore are shown in Figure 7b for comparison, i.e. the same trends are observed for d_A and d_F, and the reduced pressure of condensation decreases with temperature.

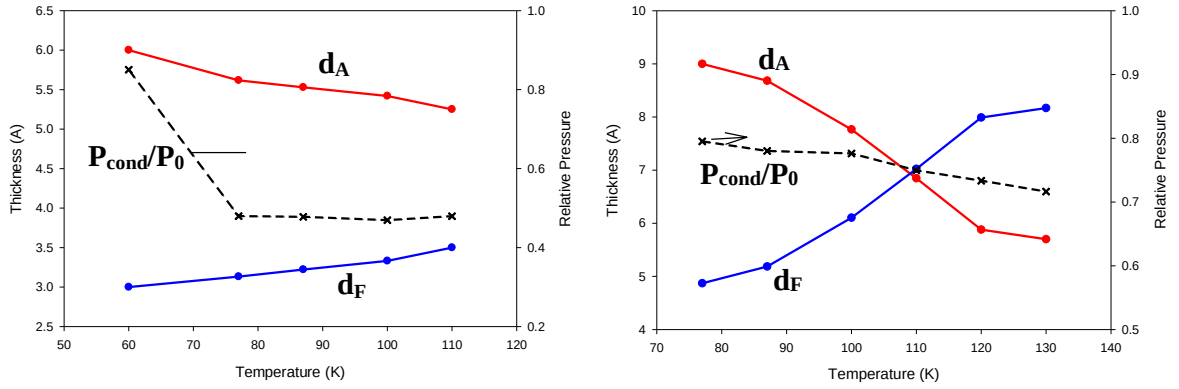

Figure 7: Plots of d_A, d_F measured on one of the pore walls and the reduced condensation pressure as a function of temperature, (a) 3 nm pore width, (b) 4 nm pore width.

Critical Hysteresis Temperature, T_{ch}

We can now define the critical hysteresis temperature, T_{ch} to be the temperature at which equation (2) is satisfied when $d_A = d_A^*$

$$[H_C = H - 2(d_A^* + d_F)]_{P_{cond}} = H_C^* \qquad (3)$$

This implies that at T_{ch} there is still a transition in the adsorbate density at the condensation pressure (which is the same as the evaporation pressure). In Figures 8a and b, the isotherm and the PNF obtained at 125 K for the 3 nm pore are presented; this temperature corresponds to T_{ch} for this pore and therefore there is no longer any hysteresis loop here, but a sharp transition is still observed. The PNF just before condensation in Figure 8b has the same pattern as those at lower temperatures. However, the fluctuation front in the central pore region where it is greater than unity is not well defined, and the difference between the particle number fluctuation at the peaks at 10 and 20 A and the core region is much smaller than at the subcritical temperatures.

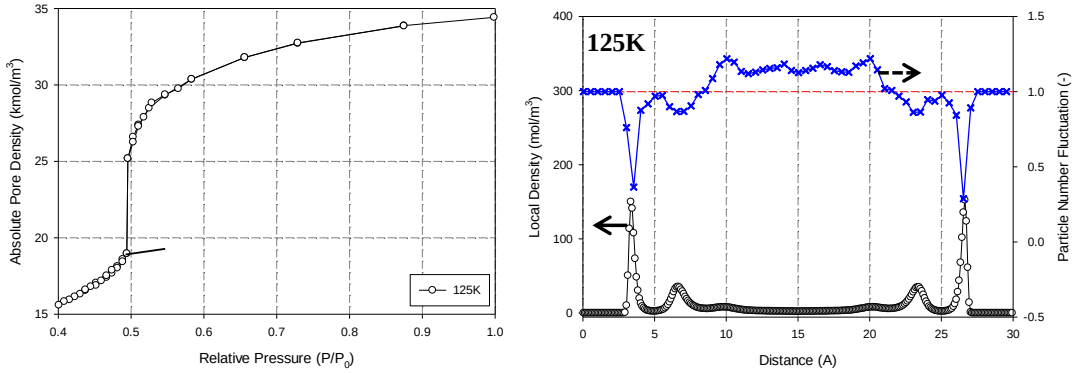

Figure 8: Argon adsorption in a slit pore of width 3 nm and length 14 nm at 125 K, (a) isotherms, (b) the density distribution and PNF just before condensation.

3.3 Critical Hysteresis Pore Size

Eq. (3) defines the critical hysteresis temperature for a given pore size. Conversely, for a given temperature it can be used to define the critical hysteresis pore size. This establishes a connection between the critical hysteresis pore size and the critical hysteresis temperature.

3.4 Effects of Pore Size

Figure 9a shows the isotherms of argon at 87 K for pores having width 3 nm, 4 nm and 5 nm and length 14 nm, and the PNFs for these pores just before condensation are shown in Figure 9b. As before, the critical core size just before condensation, highlighted by the shaded area in Figure 9b, is the same for all pore sizes. .

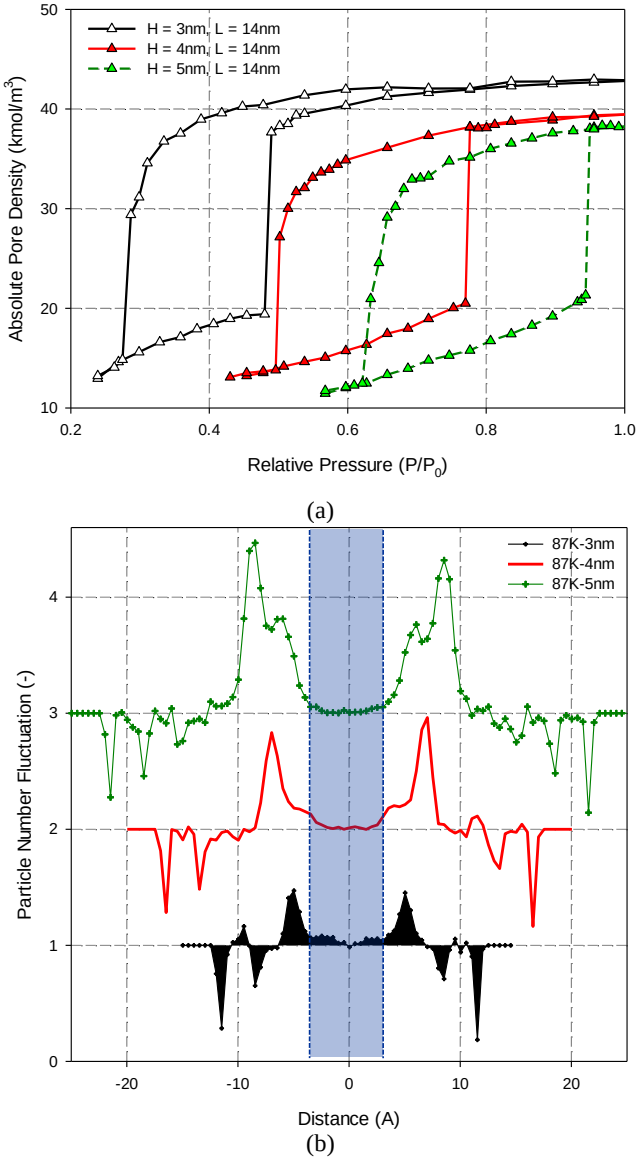

Figure 9: Adsorption isotherms of argon at 87 K in slit pores whose widths are 3, 4 and 5 nm and length is 14 nm, (a) adsorption isotherms, (b) particle number fluctuation just before condensation.

The fluctuation zone is not just a function of temperature, but also of the distance from the surface (because the solid-fluid interaction decreases with distance from the surface), and this is manifested in Figure 9 where we see that the fluctuation zone at the point just before condensation becomes larger as the pore size is increased. Figure 10a illustrates the evolution of the particle fluctuation number as a function of pressure for the points marked on the isotherm in Figure 10b for a pore of 4 nm width. The demarcation boundary of the fluctuation front is shaded in blue. Appendix 2 shows the corresponding figures for a pore of 5 nm width.

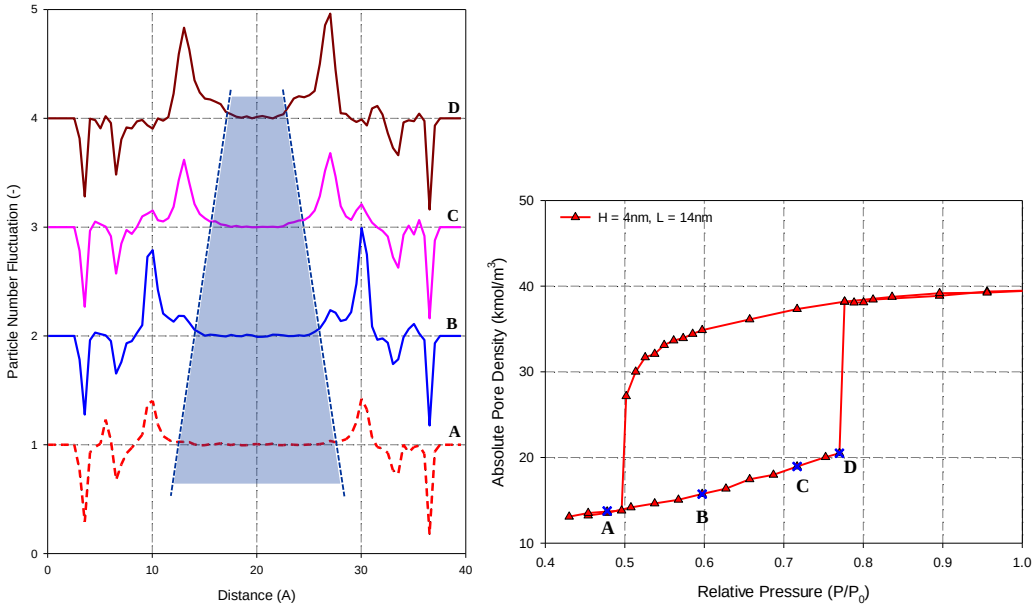

(a) (b)

Figure 10: The evolution of the particle number fluctuation with pressure for Ar adsorption at 87 K in pores of width of 4 nm. The blue cone demarks the boundary of the fluctuation front, showing the gradual narrowing as pressure, indicated on the isotherm (b), increases.

The effects of pore width on the particle number fluctuation just before condensation at different temperatures are summarized in Appendix 3.

3.5 Effects of Solid Affinity

The effects of solid affinity on the behaviour of the adsorbate before condensation are presented in Figure 11, where we show the isotherms and the PNFs just before condensation for argon adsorption at 87 K in a slit pore of width 3 nm and length 14 nm, with ε_{ss}/k reduced from 28 K to 10 K. On this weaker surface, the condensation occurs at a higher pressure as expected, and the adsorbed amount just before condensation is less; however, the plot of PNF versus distance in Figure 11b shows that the fluctuation front is identical to that

for the 28 K pore walls (i.e. the same core size), and the thickness of the fluctuation region is increased at the expense of the adsorbed layer, d_A and d_F are marked as regions I and II in the figure, respectively. As can be seen in Figure 11b, on the weaker surface since the pore walls exert less force on the fluid, there are two fluctuation peaks before the condensation, one on each side of the pore walls, compared to only one for the 28 K pore walls. The same is observed for 4 nm pore (Appendix 4).

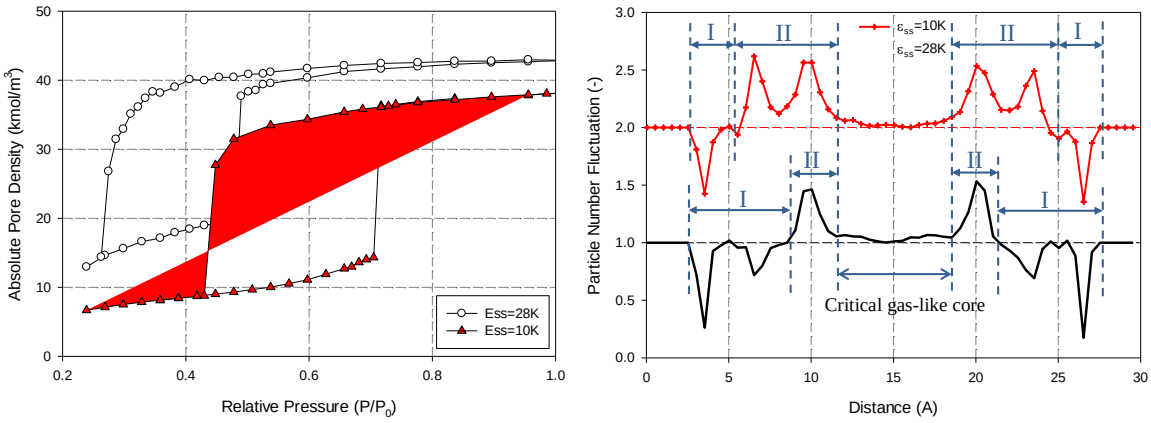

(a) (b)

Figure 11: Comparisons of (a) isotherms and (b) PNF just before condensation, for argon adsorption at 87K in a slit pore of 3nm width and 14nm length with ε_{ss}/k of the adsorbent equal to 28K and 10K, respectively.

3.6 Development of Condensation Theory

We have established a fundamental basis for capillary condensation and definitions of the critical hysteresis temperature and critical hysteresis pore size. Given eq. (1) as a definition of the core size and eq. (2) as the criterion for condensation, we need to determine d_A (the thickness of the adsorbed layer) as a function of reduced pressure and temperature and d_F (the thickness of the fluctuation layer) as a function of temperature and the distance from the surface. Since we are dealing with mesopores, where the molecular layering on one wall is not affected by the presence of the opposite wall, we can consider adsorption on a single flat surface and explore the following functional form:

$$d_A = f(P/P_0\,;T) \qquad (4a)$$

$$d_F = g(z;T) \qquad (4b)$$

It is expected that the thickness of the fluctuation zone will increase with temperature as shown in Figure 7. To confirm this we compare the particle number fluctuation, just before condensation at 87 K for slit pores with those obtained for adsorption on a flat graphite surface as shown in Figure 12. There is close agreement between the two systems, implying

that the values of d_A and d_F can indeed be determined from simulations of adsorption on a single flat surface. The results are summarized in Figure 13 where we have plotted d_A and d_F as functions of pressure at 87 K. From this graph, the condensation pressure for pores with different pore widths can be estimated. For example, for the 4 nm pore (shown as a horizontal dashed line) the reduced condensation pressure is 0.77.

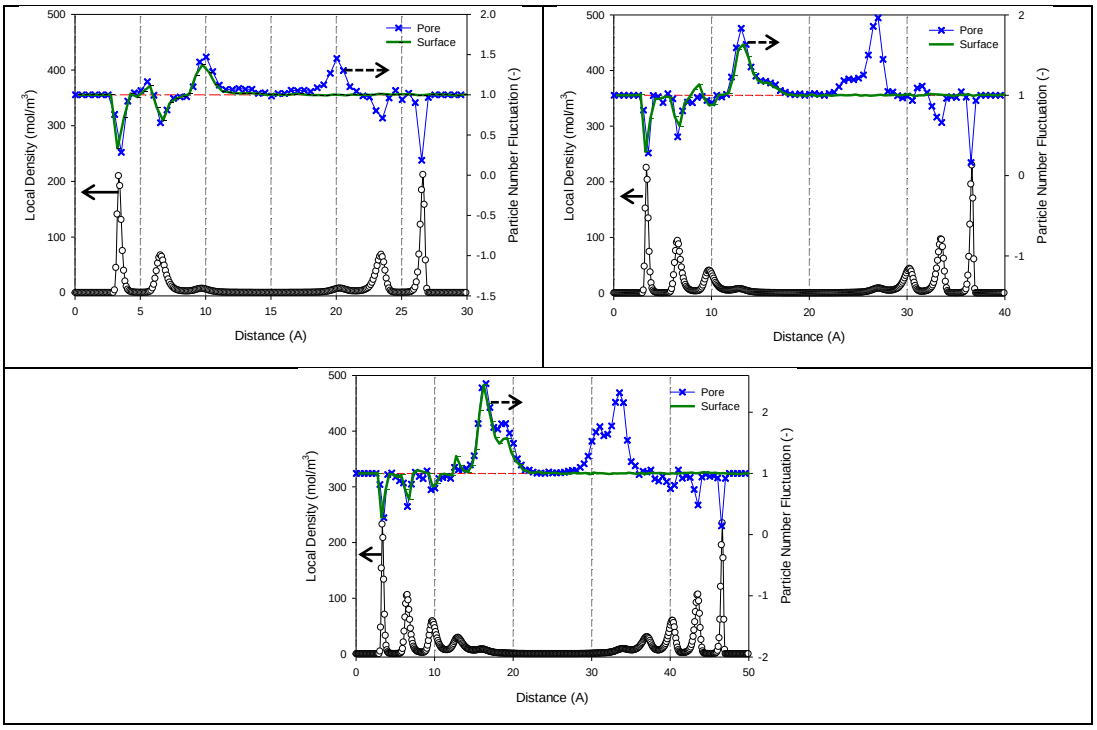

Figure 12: Comparison of particle number fluctuations just before condensation for argon adsorption at 87 K in slit pores and on a graphite surface at the same pressures; the pore size are as shown on the graphs.

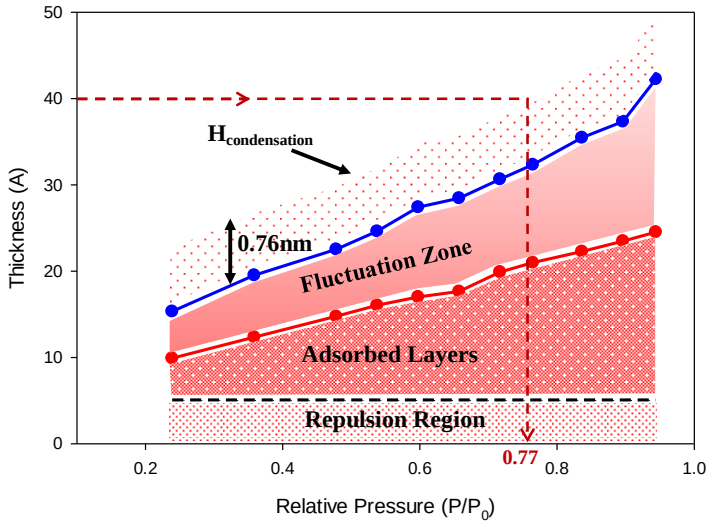

Figure 13: The values of d_A and d_F as a function of pressure for argon adsorption on a graphite surface at 87K.

In Figure 14, we show the values of d_A and d_F as a function of reduced pressure based on the PNF of argon adsorption on a graphite surface at 87 K and 110 K. As temperature is increased, we see that at the same reduced pressure, the thickness of the dense adsorbed layer decreases and the thickness of the fluctuation layer increases. As a consequence, for a given pore size, condensation occurs at a lower reduced pressure than at a lower temperature. For example, for a 4 nm pore the reduced pressure at condensation at 87 K is 0.77 while at 110 K it is 0.7.

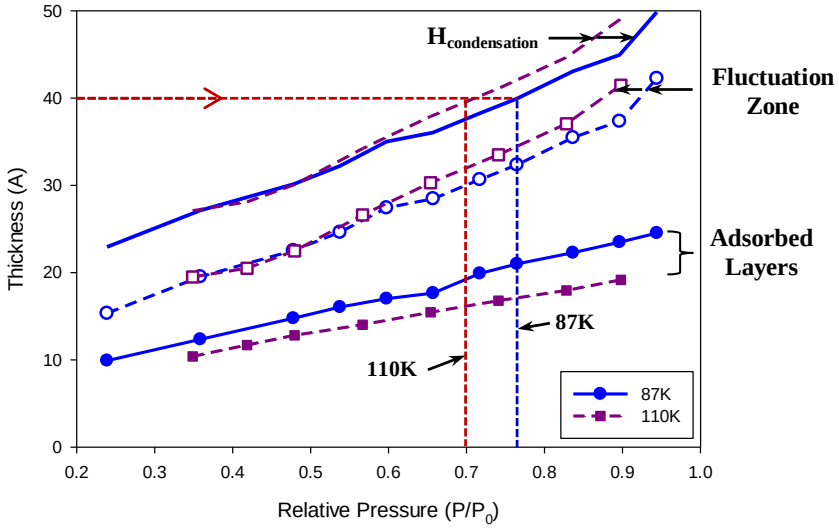

Figure 14: Comparison of d_A and d_F as a function of reduced pressure for argon adsorption on a graphite surface between 87 K and 110 K.

4. Conclusions

The theory presented here emphasises the importance of fluctuations at the boundary of the growing adsorbate layer. By measuring number fluctuations during the course of a simulation, we have been able to show that the undulations in layer structure to which they give rise, are of critical importance to the condensation process in slit pores. It is demonstrated that when gaps between the growing adsorbate layers reduce to a width where intermolecular separations at the bridges are close to the adsorbate potential minimum, condensation is nucleated. This observation has not been reported previously.

By measuring number fluctuations we have been able to identify three regions in the adsorbate: a dense region I, a more rarefied region II and a gas-like region. As adsorption proceeds I and II grow at the expense of the gas-like region. The high values of the particle fluctuation number (PNF) in II gives rise to a transient accumulation of adsorbate atoms which is manifested at the statistical level as non localised wave-like undulations in the adsorbate structure, these can be captured in snapshots and are strongly reminiscent of the thermodynamic theory proposed by Everett and Haynes [1].

The properties of the fluctuation region are dependent on temperature and on the strength of the adsorbent well depth parameter and can be deduced from independent simulations on a conjugate planar surface.

The theory gives a direct means of estimating the critical hysteresis temperature and the critical pore width.

Acknowledgement: This project is supported by the Australian Research Council

References

1. D. H. Everett and J. M. Haynes, in *Colloid Science*, ed. D. H. Everett1973, vol. 1, pp. 123-172.
2. M. Thommes, in *Nanoporous Materials, Science & Engineering* eds. G. Lu and X. S. Zhao, Imperial College Press, London2004, vol. 4, ch. 11, pp. 317-364.
3. B. Coasne, K. E. Gubbins and R. J. M. Pellenq, *Adsorption*, 2005, **11**, 289-294.
4. R. Evans, U. M. B. Marconi and P. Tarazona, *Journal of Chemical Physics*, 1986, **84**, 2376-2399.
5. C. T. Kresge, M. E. Leonowicz, W. J. Roth, J. C. Vartuli and J. S. Beck, *Nature*, 1992, **359**, 710-712.
6. D. Y. Zhao, Q. S. Huo, J. L. Feng, B. F. Chmelka and G. D. Stucky, *Journal of the American Chemical Society*, 1998, **120**, 6024-6036.
7. L. H. Cohan, *Journal of the American Chemical Society*, 1938, **60**, 433-435.
8. A. A. Schuchowitzki, *Kolloid-Zeitschrift*, 1934, **66**, 139-147.
9. B. Derjaguin, *Acta Physicochimica Urss*, 1940, **12**, 181-200.
10. J. C. P. Broekhoff and J. H. De Boer, *Journal of Catalysis*, 1967, 8-14, 15-27.
11. J. C. P. Broekhoff and J. H. De Boer, *Journal of Catalysis*, 1967, 15-27.
12. J. C. P. Broekhoff and J. H. De Boer, *Journal of Catalysis*, 1968, 368-374.
13. J. C. P. Broekhoff and J. H. De Boer, *Journal of Catalysis*, 1968, 377-390.
14. J. C. P. Broekhoff and J. H. De Boer, *Journal of Catalysis*, 1968, 391-400.
15. M. W. Cole and W. F. Saam, *Physical Review Letters*, 1974, **32**, 985-988.
16. D. H. Everett and J. M. Haynes, *Journal of Colloid and Interface Science*, 1972, **38**, 125-136.
17. L. Sarkisov and P. A. Monson, *Langmuir*, 2001, **17**, 7600-7604.
18. E. A. Ustinov and D. D. Do, *Physical Chemistry Chemical Physics*, 2012, **14**, 11112-11118.
19. J. P. R. B. Walton and N. Quirke, *Molecular Simulation*, 1989, **2**, 361-391.
20. M. Schoen, C. L. Rhykerd, J. H. Cushman and D. J. Diestler, *Molecular Physics*, 1989, **66**, 1171-1182.
21. W. J. Stroud, J. E. Curry and J. H. Cushman, *Langmuir*, 2001, **17**, 688-698.
22. U. M. B. Marconi and F. Van Swol, *Europhysics Letters*, 1989, **8**, 531-535.
23. U. M. B. Marconi and F. Van Swol, *Physical Review A*, 1989, **39**, 4109-4116.
24. R. Evans, U. M. B. Marconi and P. Tarazona, *Journal of the Chemical Society-Faraday Transactions Ii*, 1986, **82**, 1763-1787.
25. P. B. Balbuena and K. E. Gubbins, *Langmuir*, 1993, **9**, 1801-1814.
26. M. Jorge and N. A. Seaton, *Molecular Physics*, 2002, **100**, 3803-3815.
27. M. Thommes, *Annu. Rev. Nano Res.*, 2010, **3**, 515-555.
28. M. J. Bojan and W. A. Steele, *Surface Science*, 1988, **199**, L395-L402.
29. M. J. Bojan and W. A. Steele, *Langmuir*, 1989, **5**, 625-633.
30. M. J. Bojan and W. A. Steele, *Langmuir*, 1993, **9**, 2569-2575.
31. R. D. Mountain and D. Thirumalai, *Physica A (Amsterdam)*, 1994, **210**, 453-460.
32. H. E. A. Huitema and J. P. van der Eerden, *The Journal of Chemical Physics*, 1999, **110**, 3267-3274.
33. J. K. Johnson, J. A. Zollweg and K. E. Gubbins, *Molecular Physics: An International Journal at the Interface Between Chemistry and Physics*, 1993, **78**, 591 - 618.
34. M. a. Abdul Razak, V. T. Nguyen, L. F. Herrera, D. D. Do and D. Nicholson, *Molecular Simulation*, 2011, **37**, 1031-1043.
35. A. Lotfi, J. Vrabec and J. Fischer, *Molecular Physics*, 1992, **76**, 1319-1333.

Appendix 1

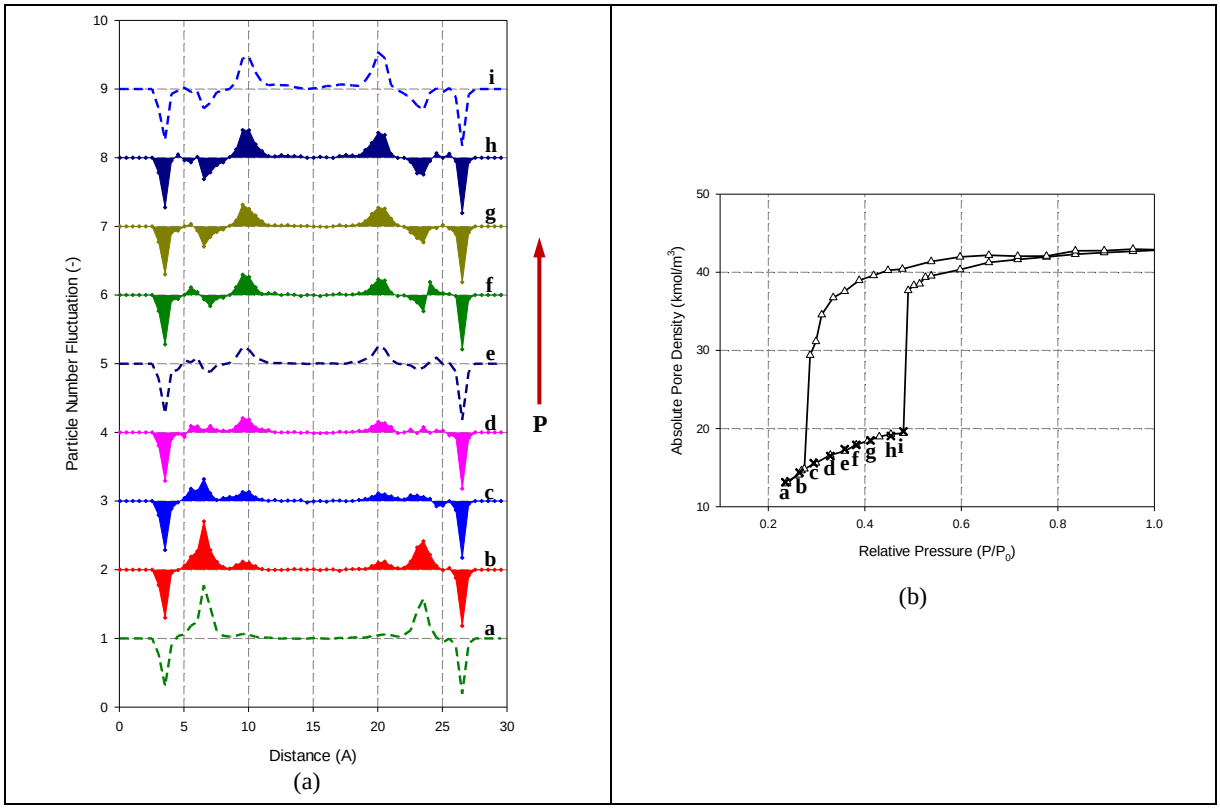

Figure A1: (a) The PNF of Ar adsorption at 87 K in slit pore of width of 3 nm and length 14 nm at different pressures points labelled on the adsorption isotherm (b) as crosses.

Appendix 2

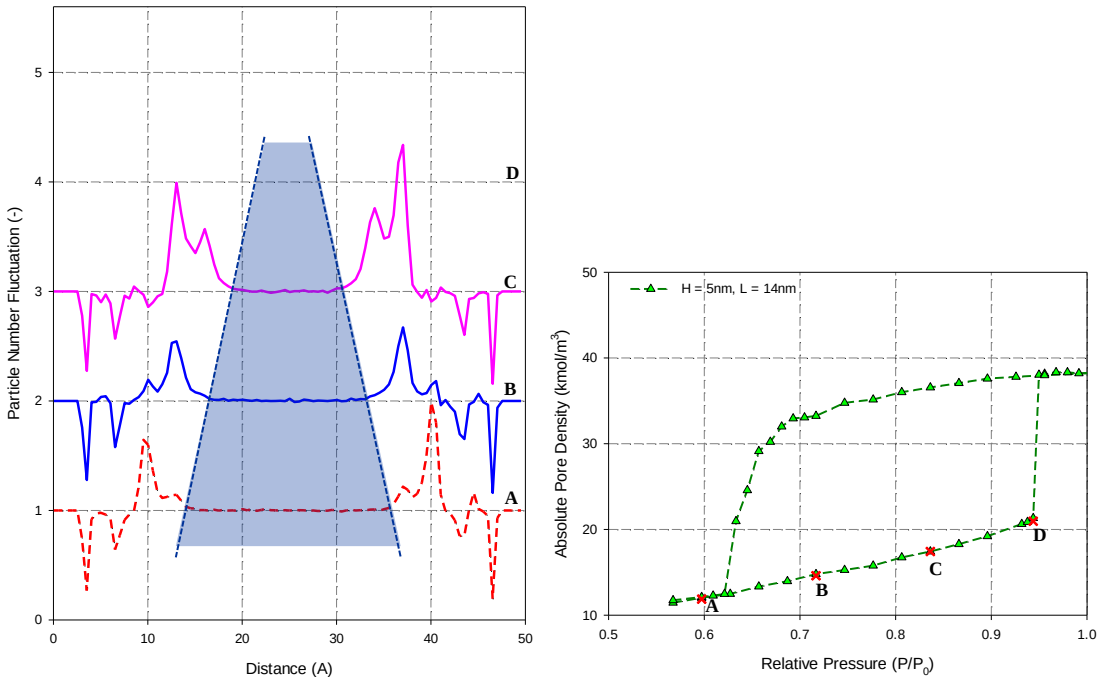

Figure A2: The evolution of the particle number fluctuation with pressure for Ar adsorption at 87 K in the pores of width of 5 nm.

Appendix 3

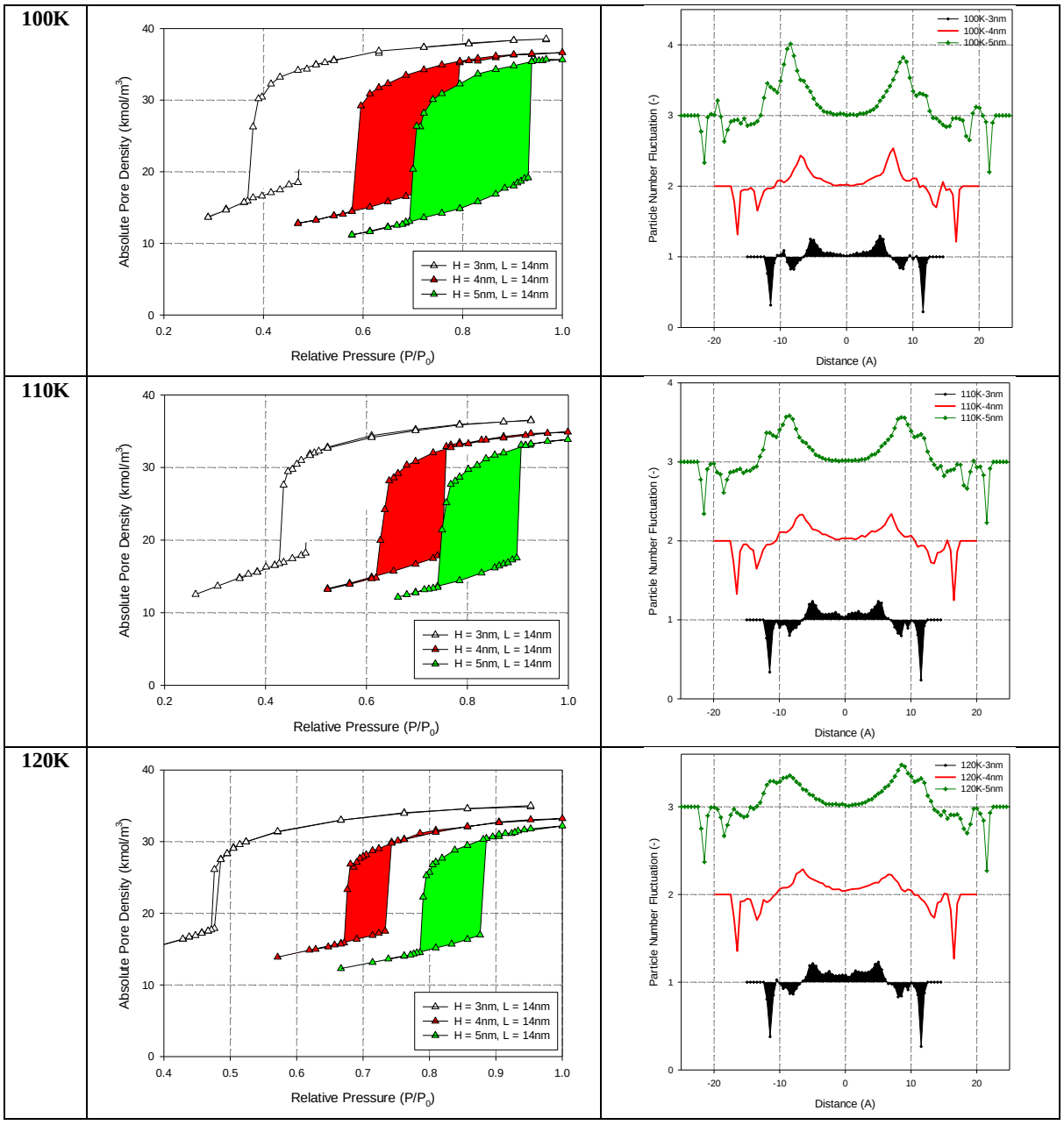

Figure A3.1: Adsorption isotherms for argon at 100 K – 120 K in slit pores whose widths are 3, 4 and 5 nm and length 14 nm, LHS: adsorption isotherms, RHS: particle number fluctuation just before condensation.

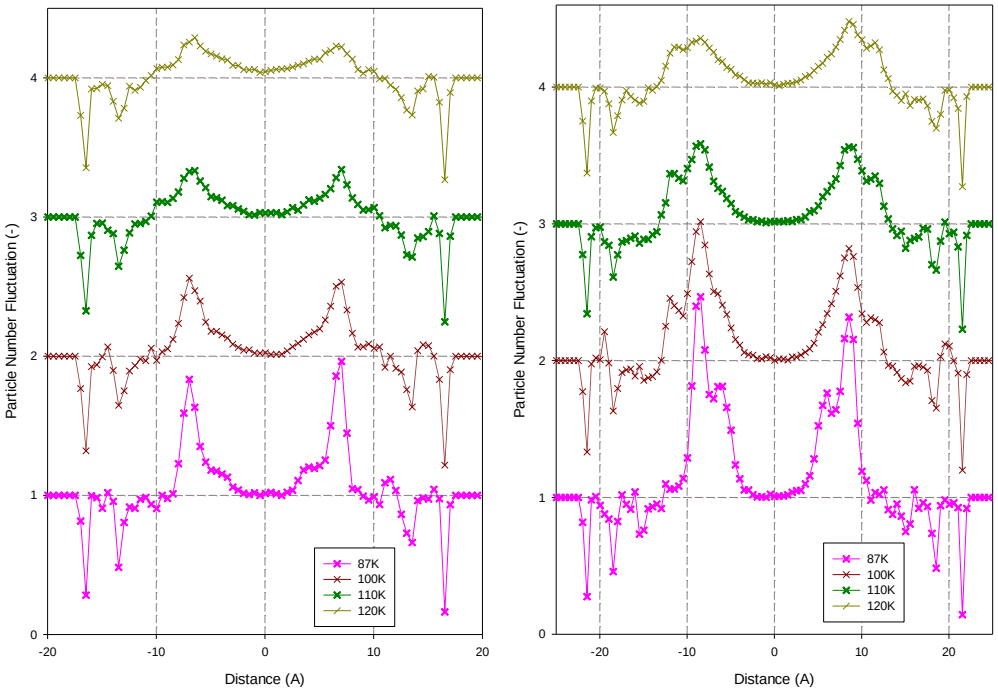

Figure A3.2: Particle number fluctuation just before condensation for argon adsorption in a slit pore whose widths are (a) 4 nm and (b) 5 nm, at different temperatures.

Appendix 4

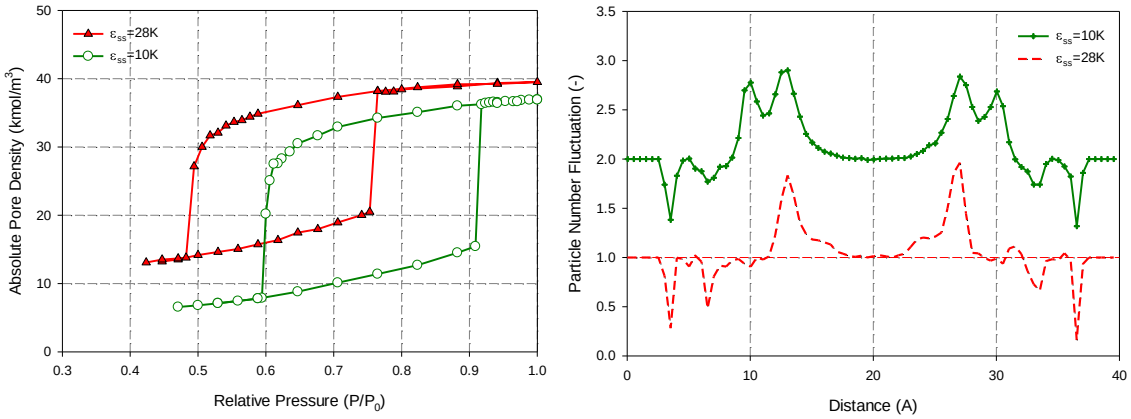

(a) (b)

Figure A4: Comparisons of (a) isotherms and (b) PNFs just before condensation, for argon adsorption at 87 K in a slit pore of pore of 4 nm width and 14 nm length, with ε_{ss}/k of the adsorbent equal to 28 K and 10 K, respectively.

Appendix 5

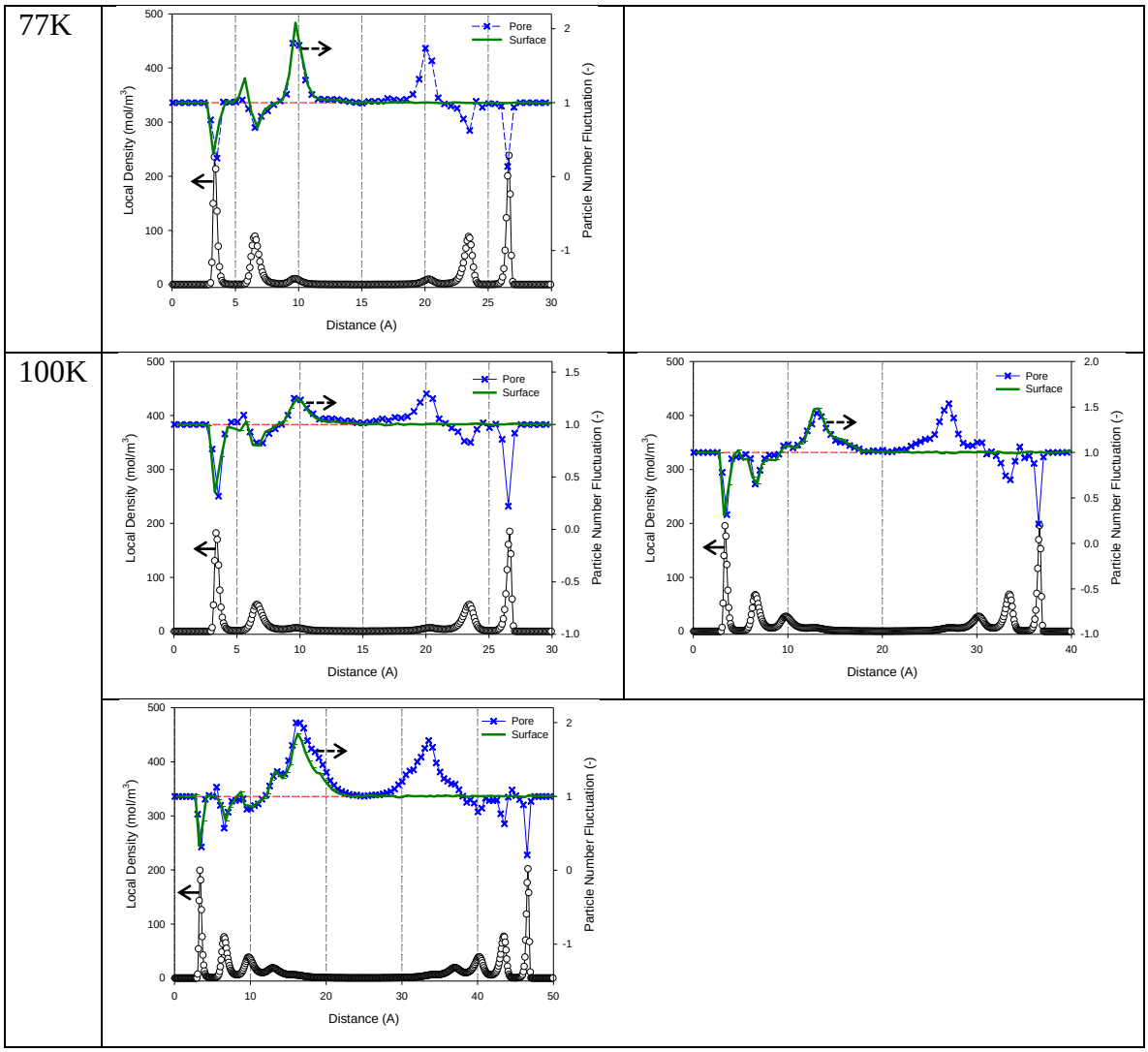

Figure A5: Comparison of particle number fluctuations just before condensation for argon adsorption in a slit pore and on a graphite surface at the same pressures; the temperatures and pore sizes are shown in the graphs.